Bull. Spec. Astrophys. Obs., 1996, 39, 101–123

Spectral atlas of the white hypergiant 6 Cas

E. L. Chentsov, F.A. Musaev, G. A. Galazutdinov

Special Astrophysical Observatory of the Russian AS, Nizhnij Arkhyz 357147, Russia

Received September 5, 1995; accepted September 20, 1995.

Abstract. A spectral atlas of 6 Cas A2.5 Ia-O and α Cyg A2 Ia, obtained in the range from 4425 to 6710Å with a spectral resolution limit of 0.15Å and S/N ratio of 100, is presented. Absorption details have been identified up to a central depth of 0.02 and equivalent width of 20 mÅ. 135 laboratory wavelength values are checked anew. Characteristic properties of the structure and kinematics of the wind of 6 Cas are illustrated.

Key words: stars: 6 Cas – atlas – line identification

1. Introduction

Creation of a star spectrum atlas is normally supposed for visual graphical presentation of a considerable portion of the spectrum and revealing maximum number of details in it. The fulfillment of this work has several reasons and variants. If a large number of spectra have been accumulated in the course of object investigation, the atlas may become its incidental final product. This is a good way of archiving observational material in a generalized form. However, the efficiency of the investigation itself can be improved by creating the atlas at its initial, preparatory stage so that processing, analysis and even acquisition of new spectra might be based on it. Moreover, new reference data, lists of lines, their effective wavelengths, etc. are attractive, because they can be used more extensively in spectroscopy of other stars of similar types. It is especially difficult to do without the atlas when one has to deal with a unique object or new observational facilities. The appearance of two spectral atlases of P Cyg (Stahl et al., 1993; Markova, 1994) in the last two years is an example where the two conditions have played a part.

This paper is also concerned with one of the brightest stars of the Galaxy, the white hypergiant 6 Cas, and its spectra taken with a CCD spectrometer and revealing some features of likeness of 6 Cas and P Cyg.

In the investigation of the structure and evolution of young star–gas–dust complexes, dynamics of stellar atmospheres and their mechanisms of loss of matter the luminous blue variables (LBV), which are inferior in luminosity only to supernovae, are still more attractive. Their light pressure on the atmospheres is so great that they are compressed occasionally to pseudophotosphere. Then part of radiation is transferred from the ultraviolet to the visible region of the spectrum, where the brightness increases several times. The spectrum of a star at this phase becomes similar to that of a white hypergiant.

Unfortunately LBV are very rare. About a dozen such objects in the Magellanic Clouds and other nearby galaxies and a few in our Galaxy, from which P Cyg is the only object in the northern sky, have been studied. Going down, with respect to luminosity, from the level of LBV to the level of hypergiants, we lose pseudophotospheres and light variations with the amplitude of 1-2 magnitude. The rest of the effects typical of LBV only weaken, and this may be compensated by the greater variety of objects and higher brightness of some of them.

6 Cas (A2.5 Ia-O, M_{bol}=-8.5^m, V=5.5^m) is a bright white hypergiant with a well pronounced instability, conveniently located in the sky. Its spectroscopic manifestation have been described by the present time quite comprehensively. The radial velocities, which are found from absorptions, show variations with both time and depth of formation of a line or even a particular part of its profile. Asymmetry is characteristic of the profiles, which is also variable and increasing with line depth. Usually the blue wing is more extended and even deepened by additional depression, i.e. absorption lines are enhanced not only by microturbulence but also by the "level effect" known in Cepheids (Aydin 1979; Sokolov and Chentsov, 1984).

Since all observable atmospheric layers move with different and variable velocities, it is important, difficult though, to find the radial velocity of the star center of mass. It has been estimated from the visual companion of 6 Cas and from its membership in the association Cas OB5. This value -44.5 km/s, falls within the interval of radial velocity variations of the deepest of the observed layers $-41 \div -53$ km/s, which

is evidence of oscillating motions in the photosphere. A characteristic duration of pulsation cycles is 1 — 1.5 months.

In the hydrogen and strongest FeII (42nd multiplet) line profiles wind components are seen. The Thomson emission wings of the Hα line extend up to $\pm$1500 km/s, the absorption part of its P Cyg profile to at least -200 km/s. In the profiles of the hydrogen and FeII (42) lines discrete absorption components are detected. They move along the broad wind absorption lines, which may be explained by the regular appearance of wind condensations, which move at acceleration outward. During 200 days individual components speed up expansion from 50 to 180 km/s (Chentsov, 1992, 1995). The phenomenon is similar to that described for P Cyg, the components are followed up to half a year, the velocity rise reaches 150 km/s (Markova and Kolka, 1988). Although not only the luminosity but also the surface temperature in P Cyg is higher, the action of some common mechanism of wind destabilization is possible.

The presented atlas of the 6 Cas spectrum and additional plots of profiles of different lines demonstrate all the above–enumerated effects. The table contains the data on the identified lines and effective wavelength used for radial velocity measurements.

2. Observational data and reduction

In the spectroscopic investigation of 6 Cas a strategy was adopted of long–term and, if possible, tight monitoring, which is similar to the strategy of the Heidelberg group of spectroscopists (Wolf et al., 1993). Such monitoring is realizable only with a moderate size telescope. We used the echelle spectrometer at the coude focus of the 1 m telescope of SAO RAS with a CCD of 520×580 pixels (Musaev, 1993). An argon–filled hollow thorium cathode lamp or the standard radial velocity star α CMi were used as the source of the comparison spectrum. To remove the traces of cosmic particles, each spectrum was exposed twice. To reduce the effect of the non–uniform sensitivity of the CCD, each spectrum was divided by the spectrum of a filament lamp ("flat field"). The attained S/N ratio was no less than 100, the spectral resolution level was 0.15 Å.

For positional measuring the line profiles, the computer matching of the original and mirror spectrum images was introduced in the program of processing CCD spectra (Galazutdinov, 1992). The dispersion curves, for each of 40 orders separately, were represented by 3rd degree polynomials with the standard deviations of the reference lines of several mÅ. Control and correction of systematic shifts of spectra were executed with the aid of the telluric lines of O_2 and H_2O. Test of radial velocities of interstellar lines and bands for their constancy were also performed. The residual systematic error for one order does not exceed $\pm$0.5 km/s.

3. Atlas, list of identified lines, and effective wavelengths

The spectra of 6 Cas and of the comparison star αCyg (A2 Ia) in the region $\lambda\lambda 4425 \div 6710$ÅÅ are presented in Figs. 1–12 as relationships between residual intensity and wavelength: the upper bold line and the lower thin one, respectively. The atlas fragments in the separate frames correspond to individual orders. The gaps between the orders appear around $\lambda \approx 4700$Å and, growing with wavelength, reach $\approx$ 22Å towards the end of the atlas. Several low–information orders were omitted. The red boundaries of the α Cyg spectrum fragments are displaced because of the slight turn of the grating. The presented curves underwent parabolic smoothing over 7 points, which had an effect only on narrow telluric lines and did not distort the stellar line profiles. The profiles displayed in Figs. 14, 15 and 16 were not subject to smoothing.

The marking–out of the horizontal axes was performed from the laboratory wavelength of rather weak absorptions. This reservation is made clear by the lower plot of Fig.14: only the lines with central residual intensities about 0.65 show one and the same radial velocity value; stronger lines yield departures from this value, which grow with their depth. The sufficiently long horizontal portion of the relationship between the radial velocity from the line core and the residual intensity was one of the criteria of selecting spectra for the atlas. Another criterion was the closeness of this constant velocity to the velocity of star mass center, which may be considered to be an idication that the inner layers of the atmosphere are relatively quiet.

Using the above criteria 2 spectra of 6 Cas, close in time (they were obtained 20 and 22.09.94), and in velocities of weak lines (about -46 and -43 km/s, respectively) have been selected for the atlas. With allowance made for the small relative shift these spectra have been averaged. The comparison star α Cyg is represented by a single spectrum taken on 15.09.94.

An atlas of the 6 Cas spectrum has once been prepared (Barsukova et al., 1989), line identification and determination of the photometric parameters have been carried out (Abbasov et al., 1972). The spectrum of α Cyg has also been described (Groth, 1961). However, the change–over from photographic plate to CCD added many new details to the already known. In clearing up their affiliation we relied upon the spectra of stars with narrow lines, such as θ Vir (A1 V) (Dobrichev and Raikova, 1989), and upon the computed synthetic spectrum in which the lines were actually not broadened. Since our objective was not

the simulation of observations but only identification of the weakest lines, for the computation we used a model atmosphere ($T_{eff} = 9000K, lgg = 1.5, [z] = 0$, ξ_{turb} = 5 km/s) from Kurucz's models list (1979), which was closest in physical parameters, and his program SYNTH adopted by V.V. Tsymbal for a personal computer IBM PC. An example of comparing the computed and observed spectra is presented in Fig. 13.

The identification of the absorption lines of the star spectrum was brought to at least a central depth of 0.02 and equivalent width of 20 mÅ. The identification results are tabulated in Table 1. The horizontal straight lines in the table demarcate the clearly distinguishable details: separate lines and their groups forming blends.

Interstellar dust bands were sought using Herbig's (1973) list. Note the uncertainty in revealing the broadest and most shallow of them in the echelle spectrum. In the atlas the interstellar details are shown above the spectrum of 6 Cas, where they are much stronger than in the spectrum of α Cyg. On the contrary, the telluric lines (marked with dots in the atlas) are especially pronounced in the spectrum of α Cyg, even the weakest H_2O line groups in the regions λ5450Å and λ5050Å are readily identified.

Only those lines are identified in the atlas, which have been used for radial velocity measurements. In Table 1 their laboratory wavelengths, including effective, are presented with two or three decimal digits. They are taken from the list of standard wavelengths for white supergiants of Dobrichev et al. (1986) as well as from the tables of Striganov and Odintsova (1982), or from the tables of solar spectra (Pierce and Breckinridge, 1973). In the last case they were taken with the corrections for the gravitational redshift. All 135 values were checked anew when measuring 11 spectra of 6 Cas, 3 spectra of α Cyg and 2 of ν Cep (A2.4 Ia). For each of these spectra was registered the radial velocity deviation for a given line from the mean relation (V_r — r), some specimens of which can be seen in Figs.14 and 15. When the deviation proved to be systematical, appropriate corrections were introduced.

4. Characteristic properties of 6 Cas and its variations with time

Thanks to the high quality of observational data the atlas detects readily the difference between 6 Cas and α Cyg not only from luminosity (lines H_α and FeI in Fig.4) but also from temperature (HeI lines in Figs. 1,4,5,9). Absorption lines in the spectra of the hyper- and supergiants are close in width but they differ considerably in profile shape. While even the strongest FeII lines remain symmetric in the spectrum of α Cyg, in the spectrum of 6 Cas they (especially clearly the line FeII 5169 Å) show P Cyg characteristic features of line profiles: pronounced blue shifts of the cores, steep red slopes of absorptions, which transform to weak emissions, extended depressions in the blue wings. The same type of depression is followed in weaker lines as well.

In Figs. 14, 15 the information on the absorption lines of the photosphere and the wind base of 6 Cas is presented in two ways: as radial velocity variation for the line core with central residual intensity and as line profile variation with its strengthening. Besides, when comparing the presented plots for different spectra one can see kinematic and profiles to be variable with time. In order that the shape of the profiles be drawn more reliably, each of the profiles was obtained as the mean for several lines FeII of identical intensity. To the four profiles, from the shallowest to the deepest, correspond the followig 4 groups of lines: $\lambda\lambda$ 4455, 5292, 5387 ÅÅ, $\lambda\lambda$ 5101, 5284, 5535 ÅÅ, $\lambda\lambda$ 4508, 4629 ÅÅ, $\lambda\lambda$ 5018, 5169 ÅÅ.

In the previous section it has been noted that the atlas includes the spectra of 6 Cas being in a relatively quiet state. Directing our attention to Fig.14 once again we see well that on 20-22.09.94 the inner atmosphere layers alone were quiet with respect to the center of mass of the star and to one another, while the outer layers were moving with acceleration outward. That is, in the lines FeII a hypergiant may show the effect of the same nature and magnitude that the Balmer progress in supergiants does. By analogy one could speak here about the "iron progress". This brings us from the photosphere to the wind base. The purely wind depressions are seen on the blue wing of the averaged profile of FeII (42) lines, the weaker one in the region 100 km/s and the stronger one near 150 km/s (goes beyond the graph). Both of them are the traces of the same condensations moving through the wind, which manifest themselves more distinctly in the blue–shifted discrete components of H_β and H_α, respectively.

Our spectral monitoring has not allowed us to follow the oscillations of the photospheric layers of 6 Cas with the desired time resolution, and in Fig.15 are compared the situations referring to different cycles. It is only seen that both increase the interval of velocity variations (from 4 to 12 km/s) and the variations of the profile shape. By comparing Fig.15 and Fig.16 it is difficult to follow the direct phase correlation of motions in the photosphere and in the wind. The situation of 8.10.93 is especially expressive: expansion deceleration in the photospheric layers, compression at the wind base and ejection with growing velocity of extremely powerful wind condensations, possibly even envelopes. In Fig.16 one can fairly see the systematic shift of the discrete components along the basic wind absorption of H_α. They are the strongest

on 8.10.93. Such a splitting of the profile has been noticed in 6 Cas only once so far (Mc Kellar, 1939).

The structure of NaI lines in the spectrum of 6 Cas is rather complex. We isolate clearly the components with velocities -56. -31, -19, +10 and +24 km/s, wich quite satisfactorily agrees with the etalon data of Hobbs (1979). The main components, -19 and -56 km/s, are interstellar, they correspond to the local and Perseus arms. The contribution of the latter to the dust bands is very small: the mean radial velocity from the sharpest of them is also -19 km/s. The short–wave component is possible to contain the stellar part as well. The best way of its isolation would be to obtain an extraatmospheric high–dispersion spectrum of the visual companion of 6 Cas.

Support for this work was provided by RFFR through Grant No. 95-02-04276-a.

References

Abbasov G.I., Zeinalov S.K., Chentsov E.L.: 1972, Astrofiz. Issled. (Izv.SAO), **4**, 81.

Aydin C.: 1979, Astrophys. Space Sci., **64**, 481.

Barsukova E.A., Lebedeva I.A., Chargeishvili K.B., Chentsov E.L.: 1983, Astrofiz. Issled. (Izv. SAO), **16**, 34.

Bartaya R.A., Chargeishvili K.B., Chentsov E.L., Shkhagosheva Z.U.: 1994, Bull. Spec. Astrophys. Obs., **38**, 103.

Chentsov E.L.: 1992, in: Atmospheres of Early–Type Stars, eds.: Huber and Jeffery (Lecture Not. in Phvs., No. 401), 128.

Chentsov E.L.: 1995, Astrophys. Space Sci., in press.

Dobrichev V., Chentsov E.L., Shkhagosheva Z.U.: 1986, Astrofiz. Issled. (Izv. SAO), **22**, 59.

Dobrichev V. and Raikova D.: 1989, Astrophys. Invest. of Bulgarian AS, **5**, 101.

Galazutdinov G.A.: 1992, Preprint SAO RAS, 92.

Groth H.G.: 1961, Zeitschr. für Astrophys., **51**, 206.

Herbig G.H.: 1975, Astrophys. J., **196**, 129.

Hobbs L.M.: 1979, Publ. Astr. Soc. Pacific, **91**, 690.

Kurucz R.L.: 1979, Astrophys. J. Suppl. Ser., 40.

Markova N. and Kolka I.: 1988, Astrophys. Space Sci., **141**, 45.

Markova N.: 1994, Astron. Astrophys. Suppl. Ser., **108**, 561.

Mc Kellar A.: 1939, Publ. American Astron. Soc., **9**, 266.

Musaev F.A.: 1993, Pis'ma Astron. Zh., **19**, 776.

Pierce A. K. and Breckinridge J. B.: 1973, Contr. Kitt Peak Nat. Obs., No. 559.

Sokolov V. V. and Chentsov E.L.: 1984, Astrofiz. Issled. (Izv. SAO), **18**, 8.

Stahl O., Mandel H., Wolf B., Gang Th., Kaufer R., Szeifert Th., Zhao F.: 1993, Astron. Astrophys. Suppl. Ser., **99**, 167.

Striganov A.R. and Odintsova G.F.: 1982, Spectral line tables of ions and atoms, Moscow, Energoizdat.

Wolf B., Mandel H., Stahl O., Kaufer A., Szeifert Th., Gang Th., Gummersbach C.A., Kovach J.: 1993, The Messenger ESO, No. 74, 19.

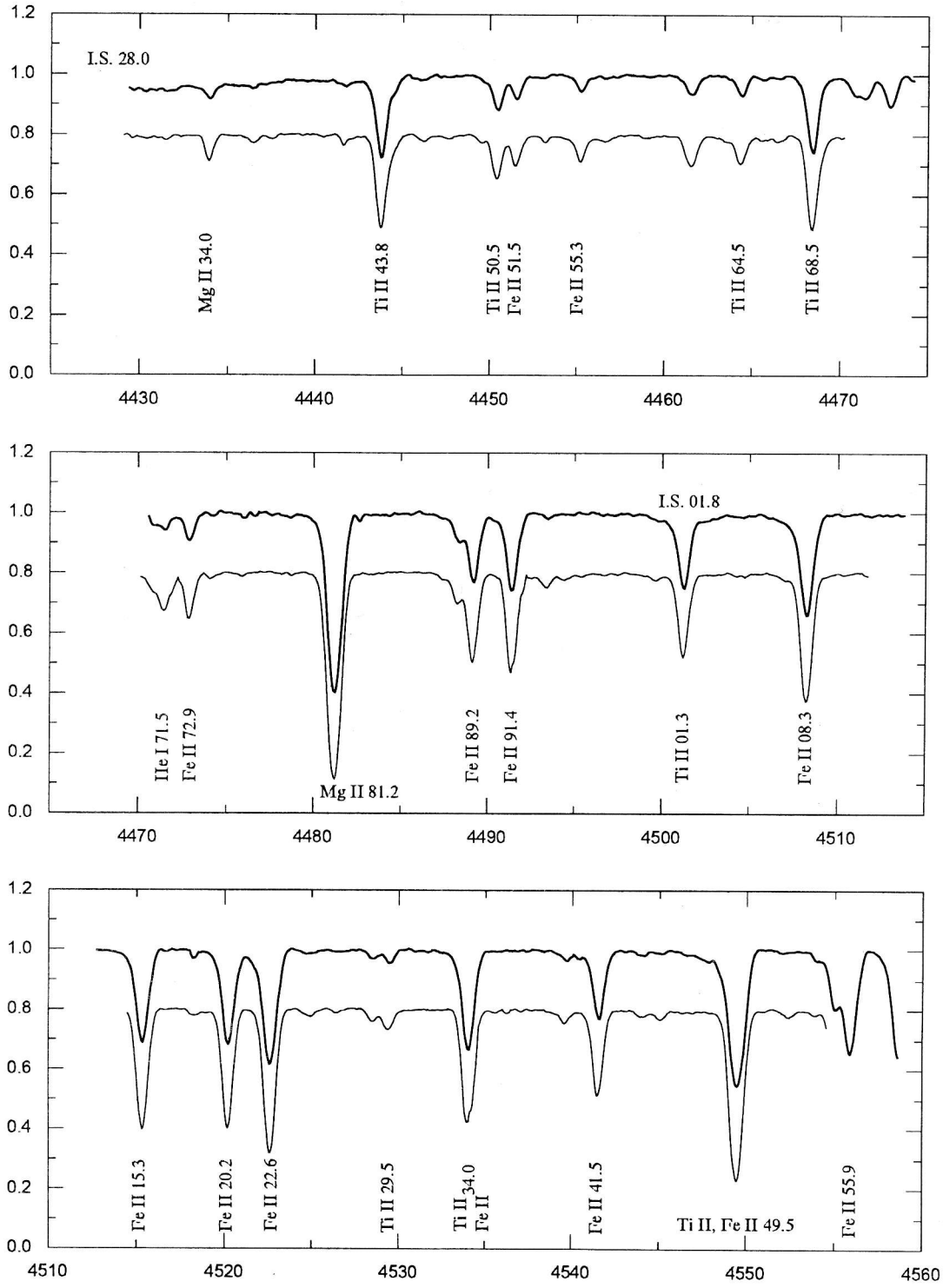

Fig.1 The spectral atlas from 4425 to 4560 A

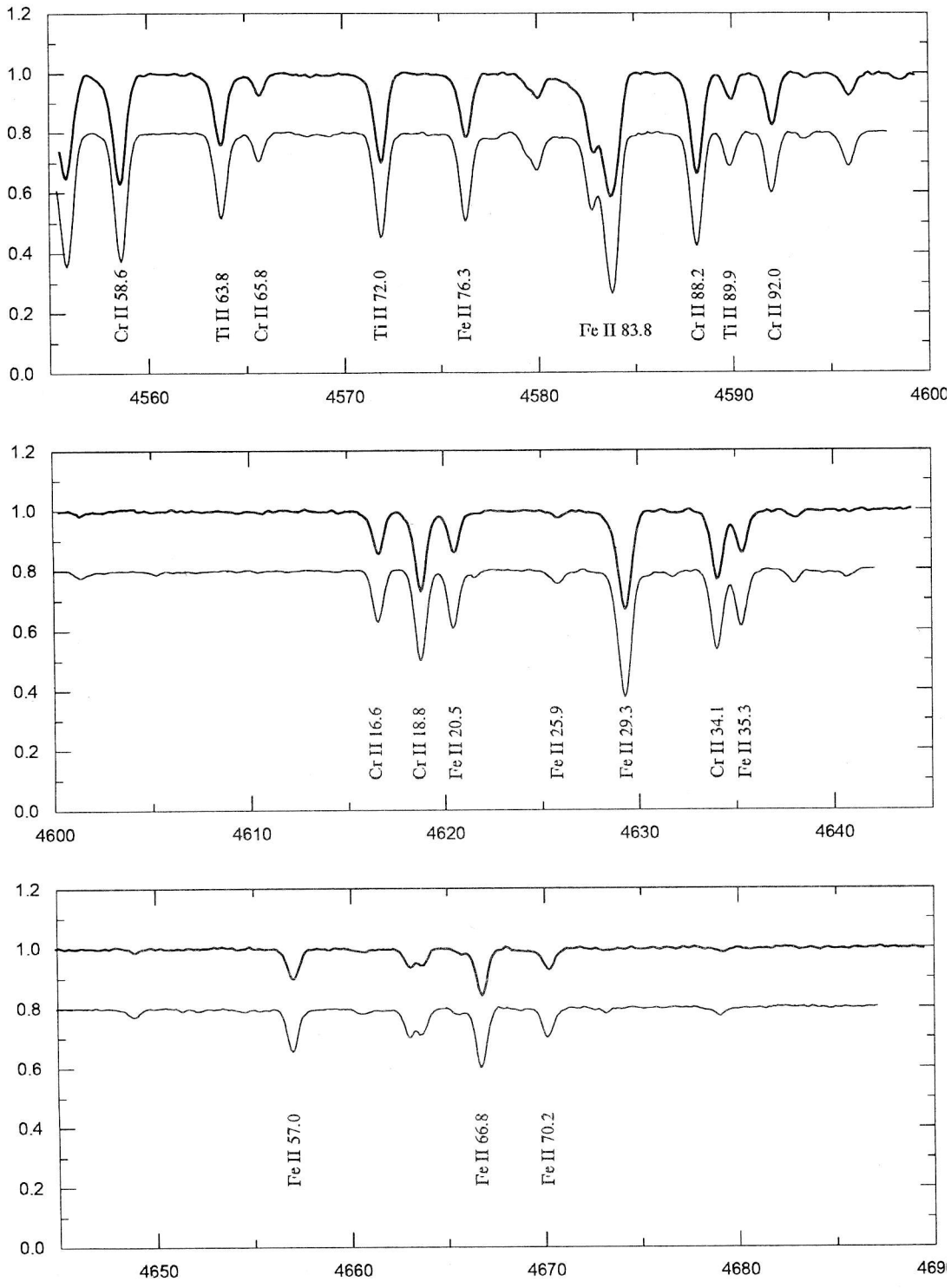

Fig.2 The spectral atlas from 4555 to 4690 A

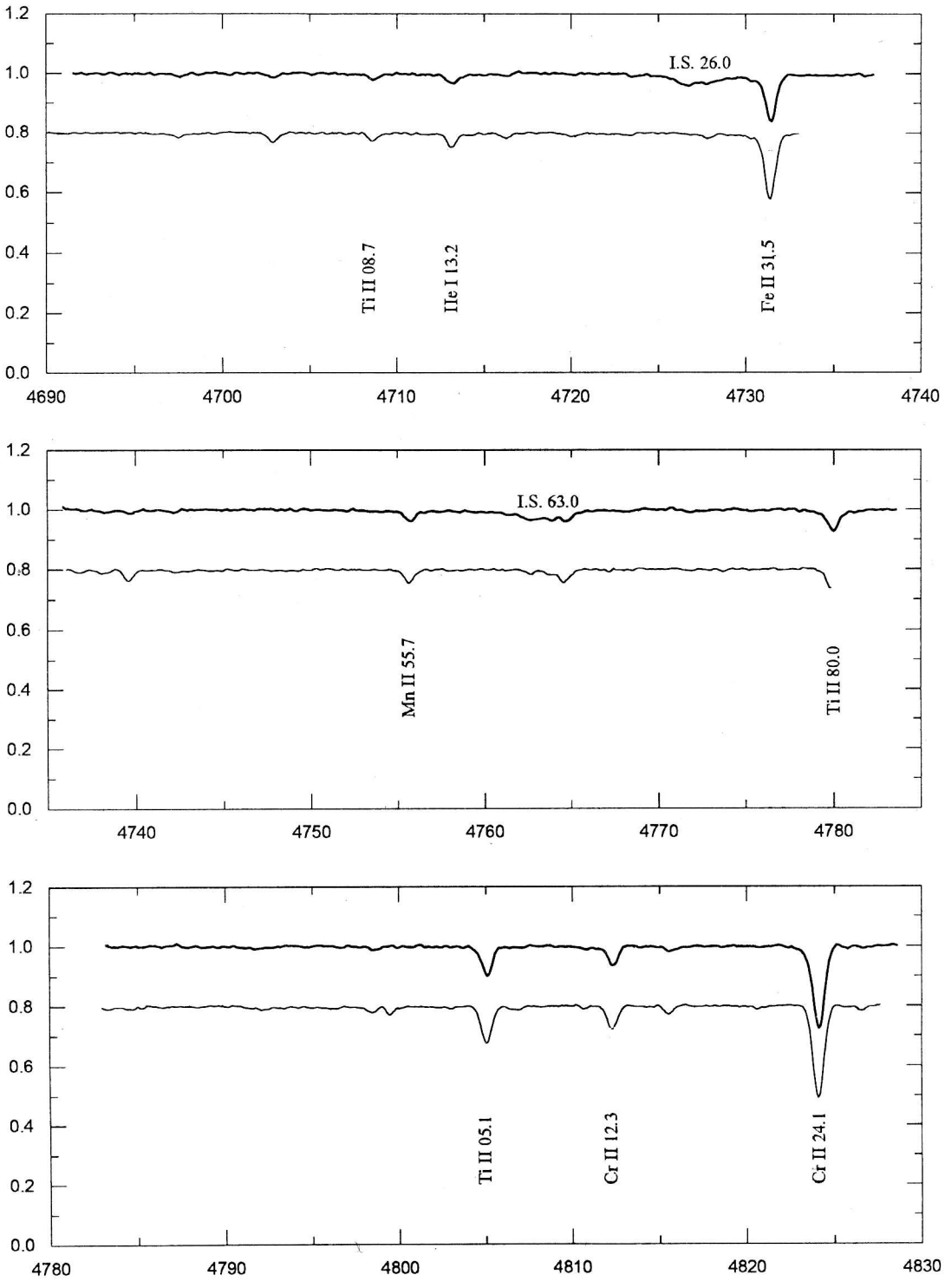

Fig.3 The spectral atlas from 4690 to 4830 A

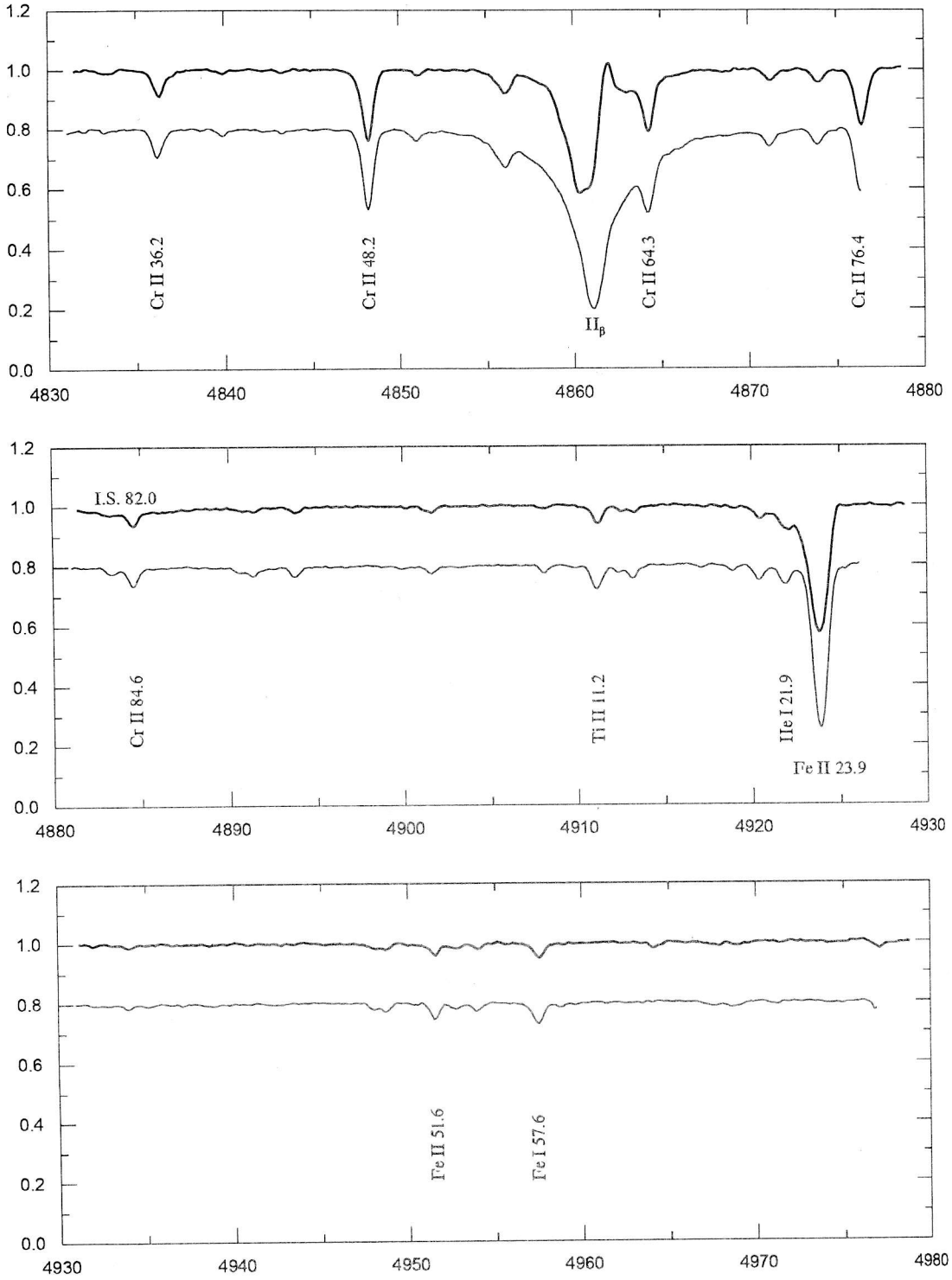

Fig.4 The spectral atlas from 4830 to 4980 A

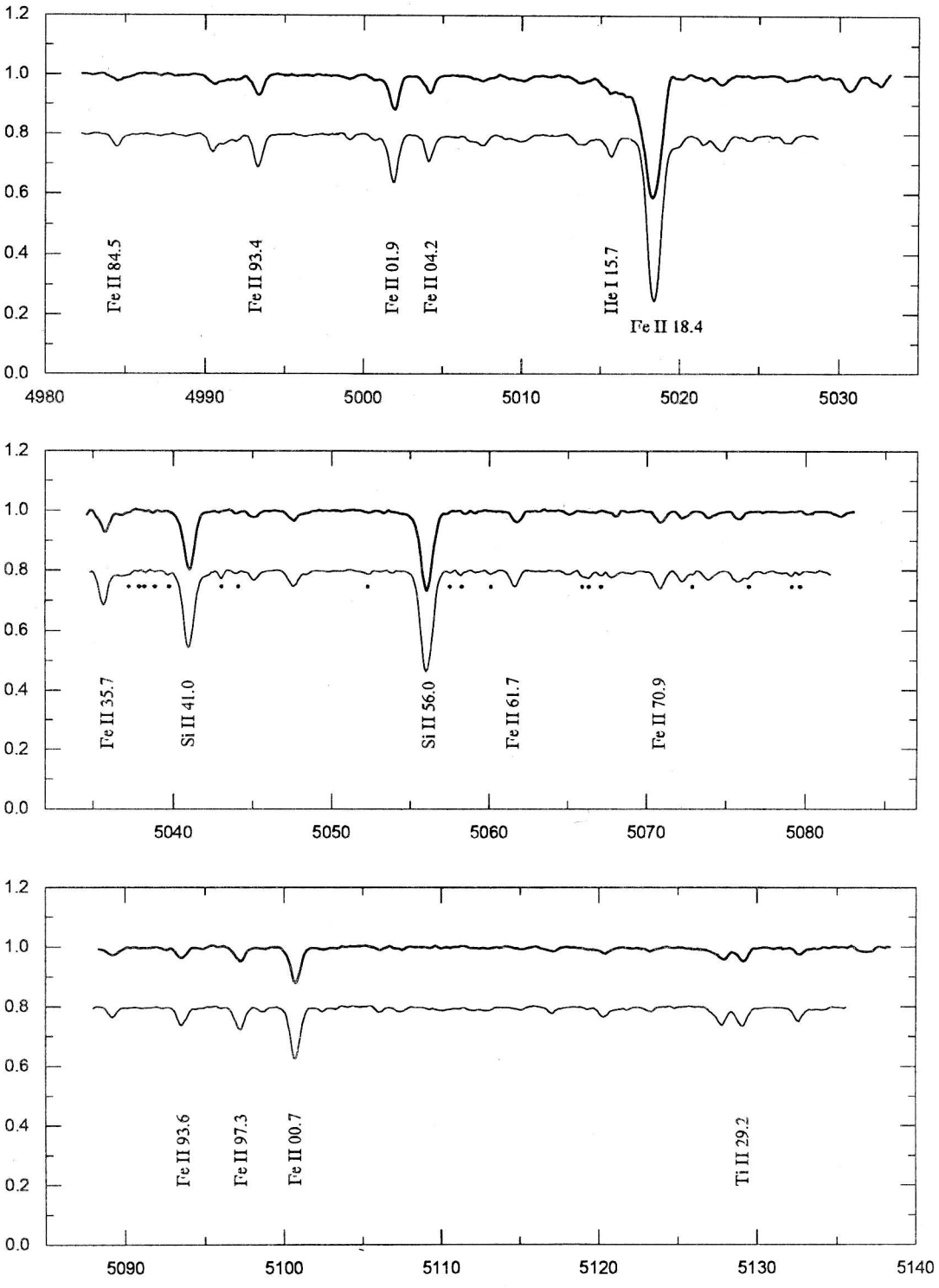

Fig.5 The spectral atlas from 4980 to 5140 A

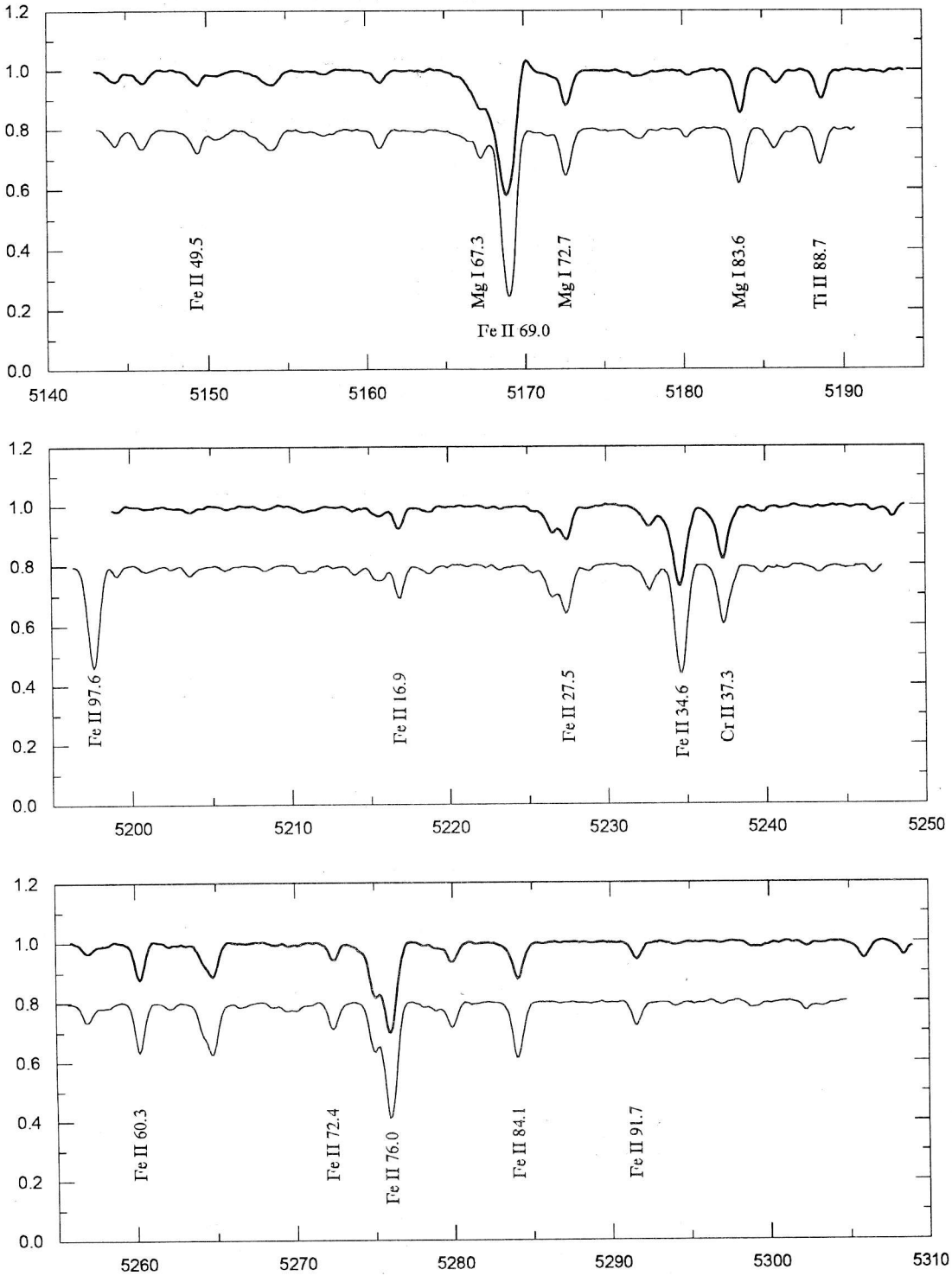

Fig.6 The spectral atlas from 5140 to 5310 A

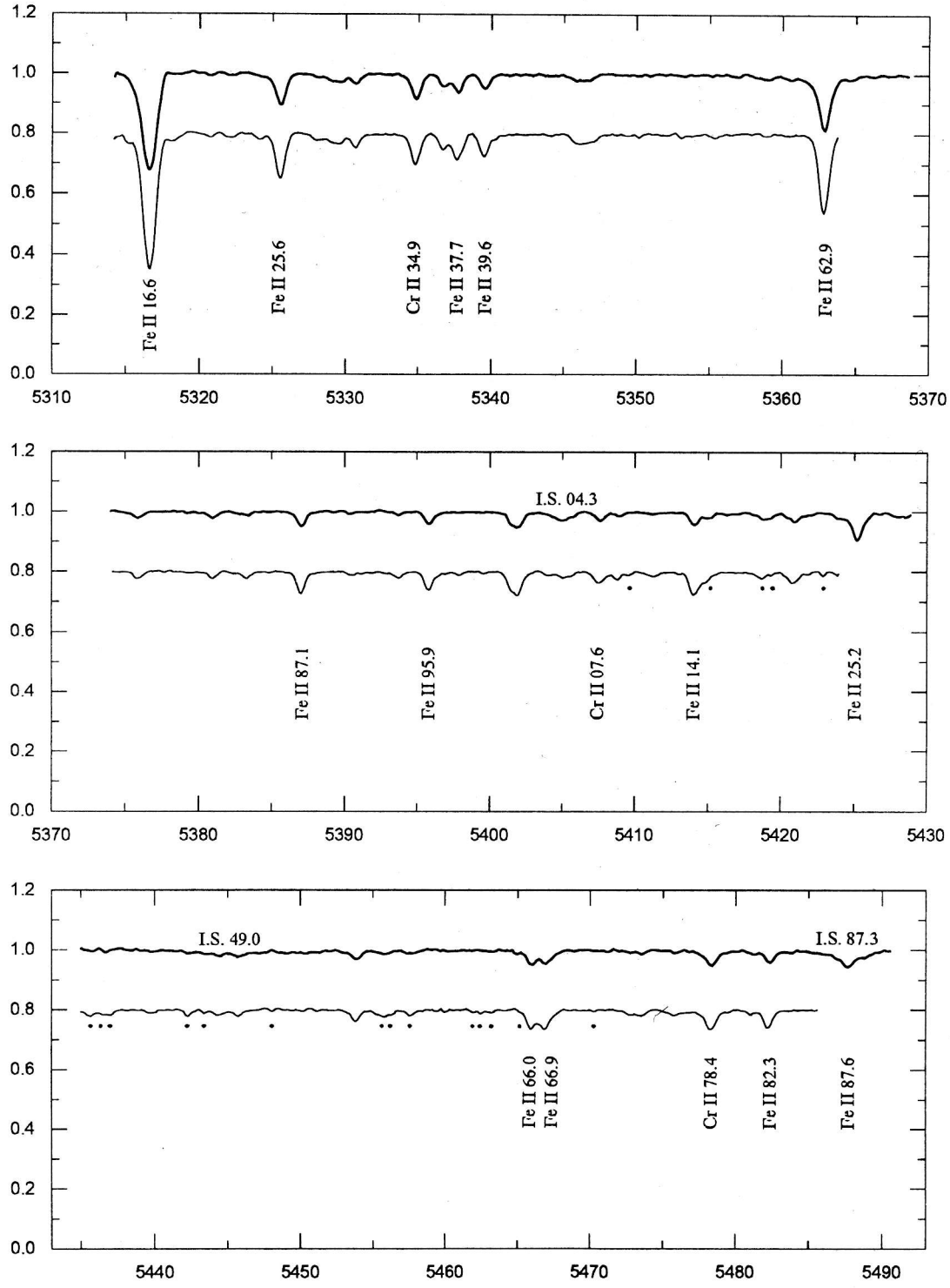

Fig.7 The spectral atlas from 5310 to 5493 A

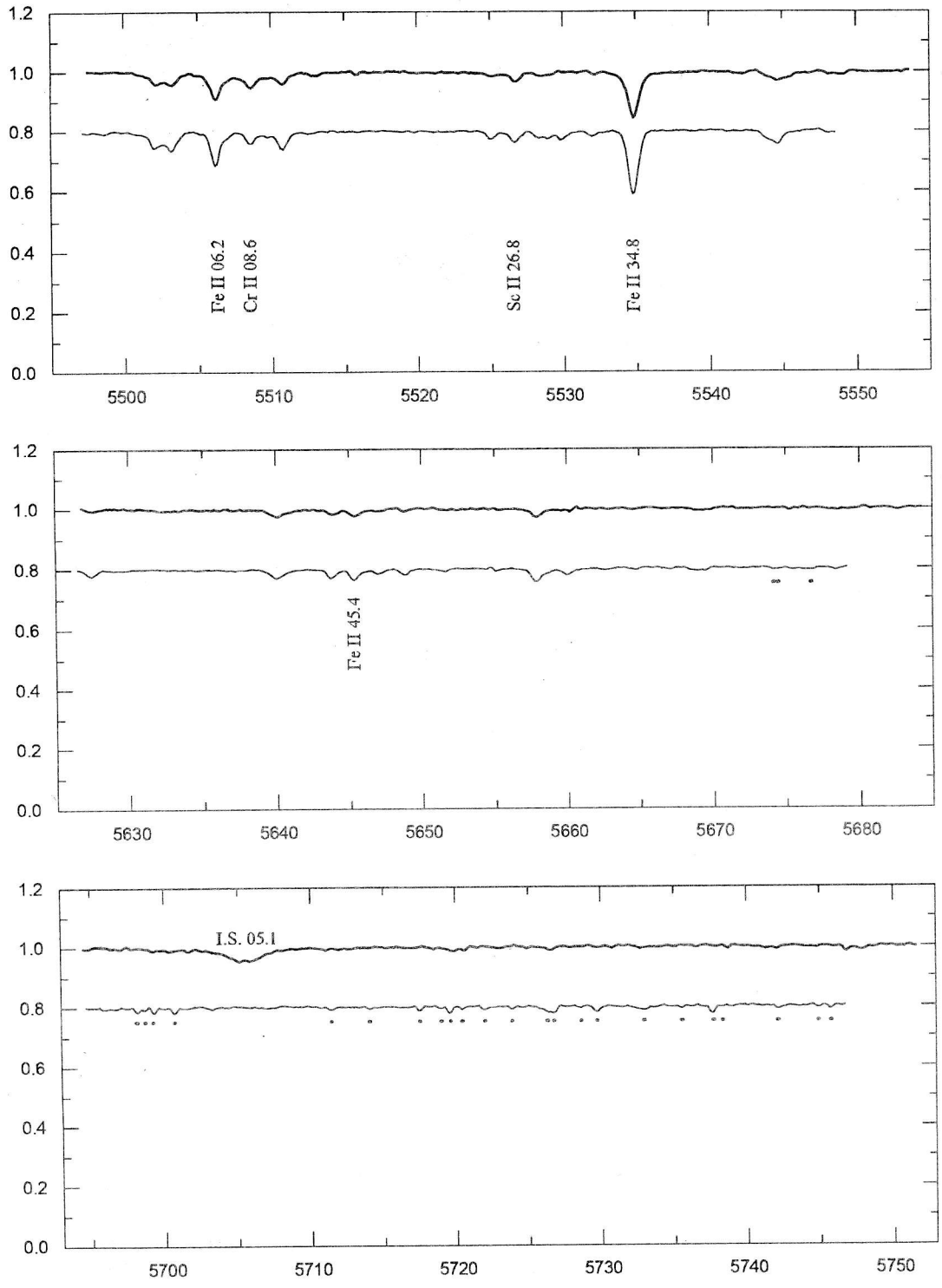

Fig.8 The spectral atlas from 5495 to 5753 A

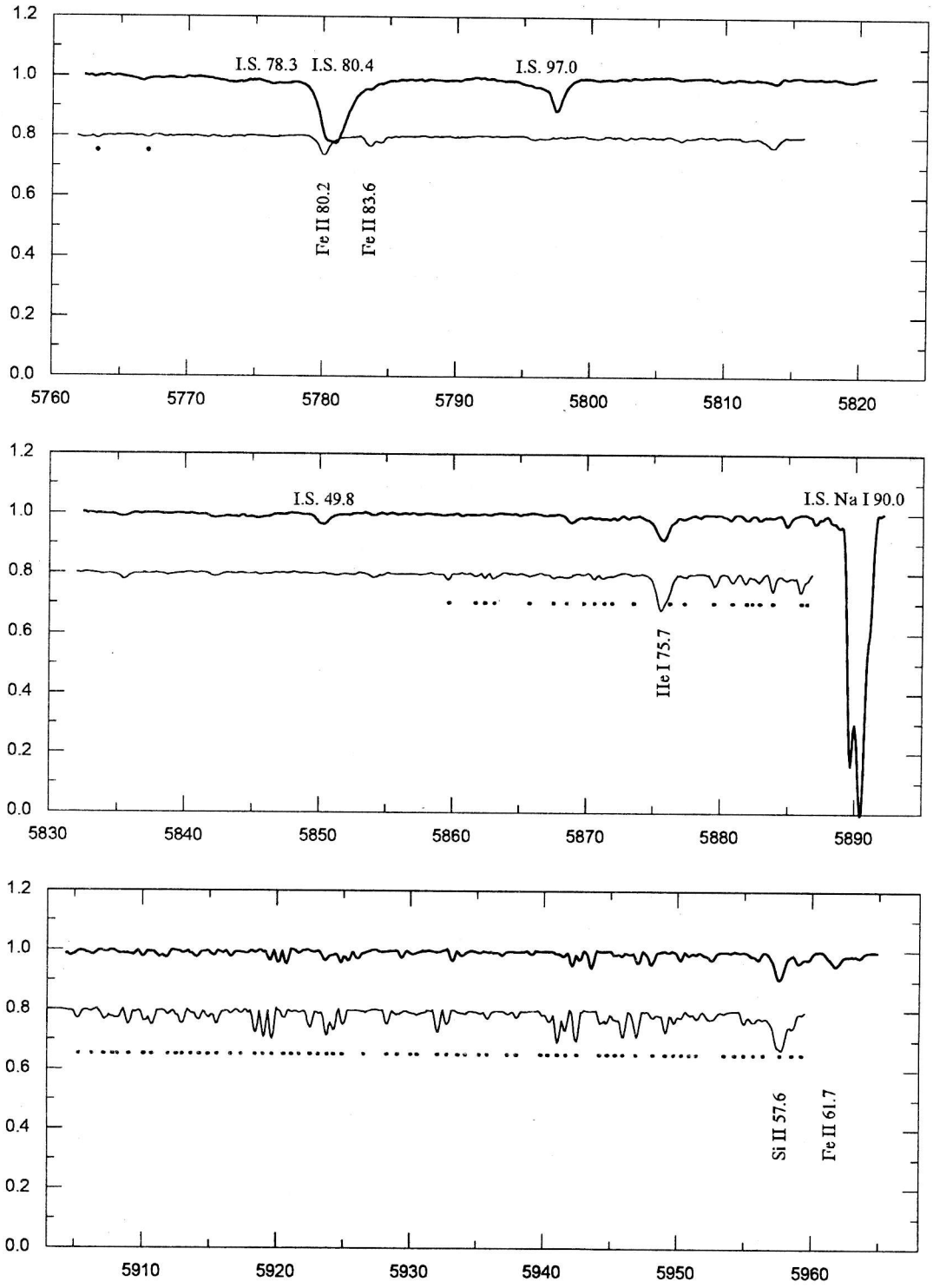

Fig.9 The spectral atlas from 5760 to 5968 A

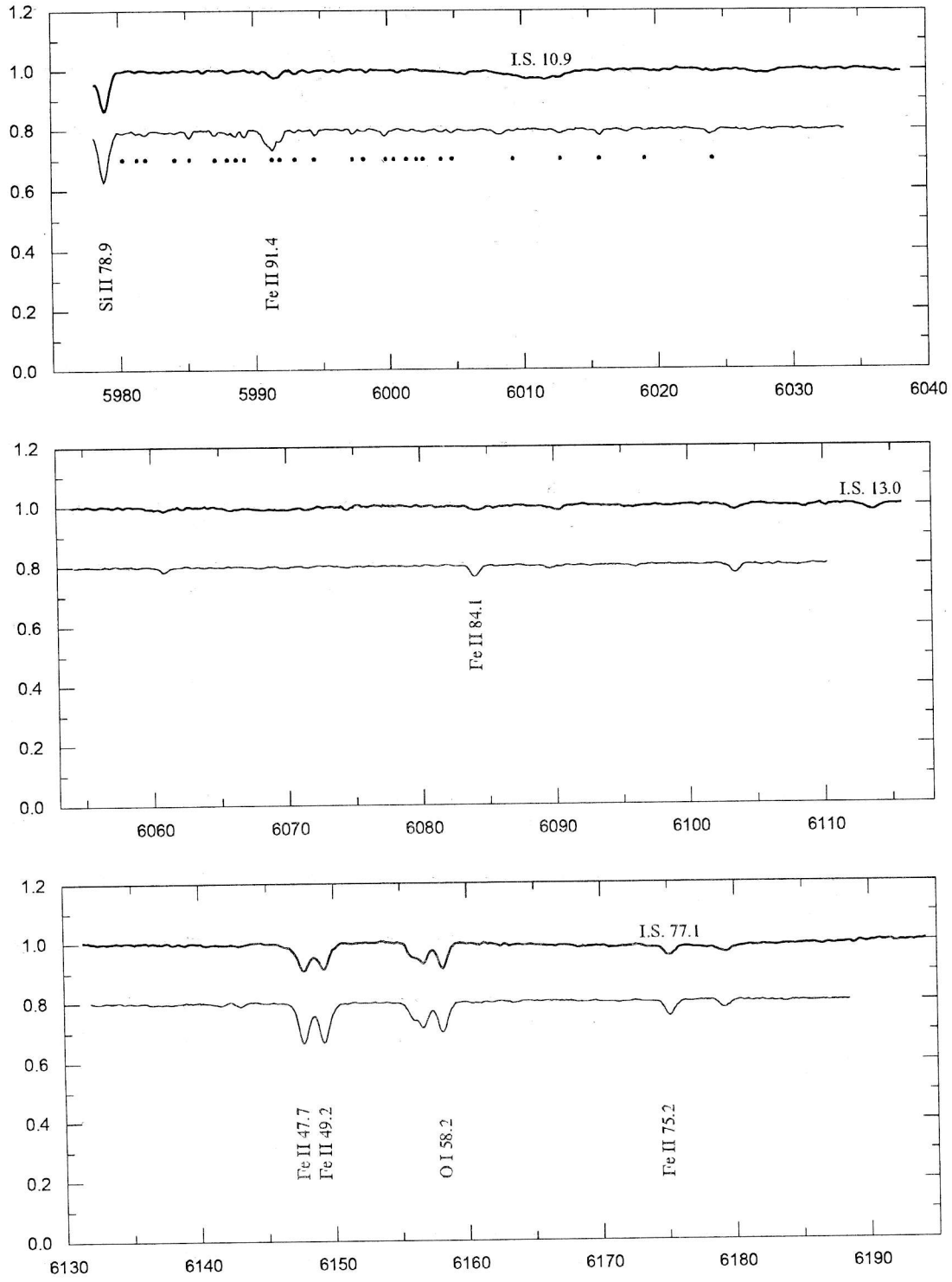

Fig.10 The spectral atlas from 5975 to 6195 A

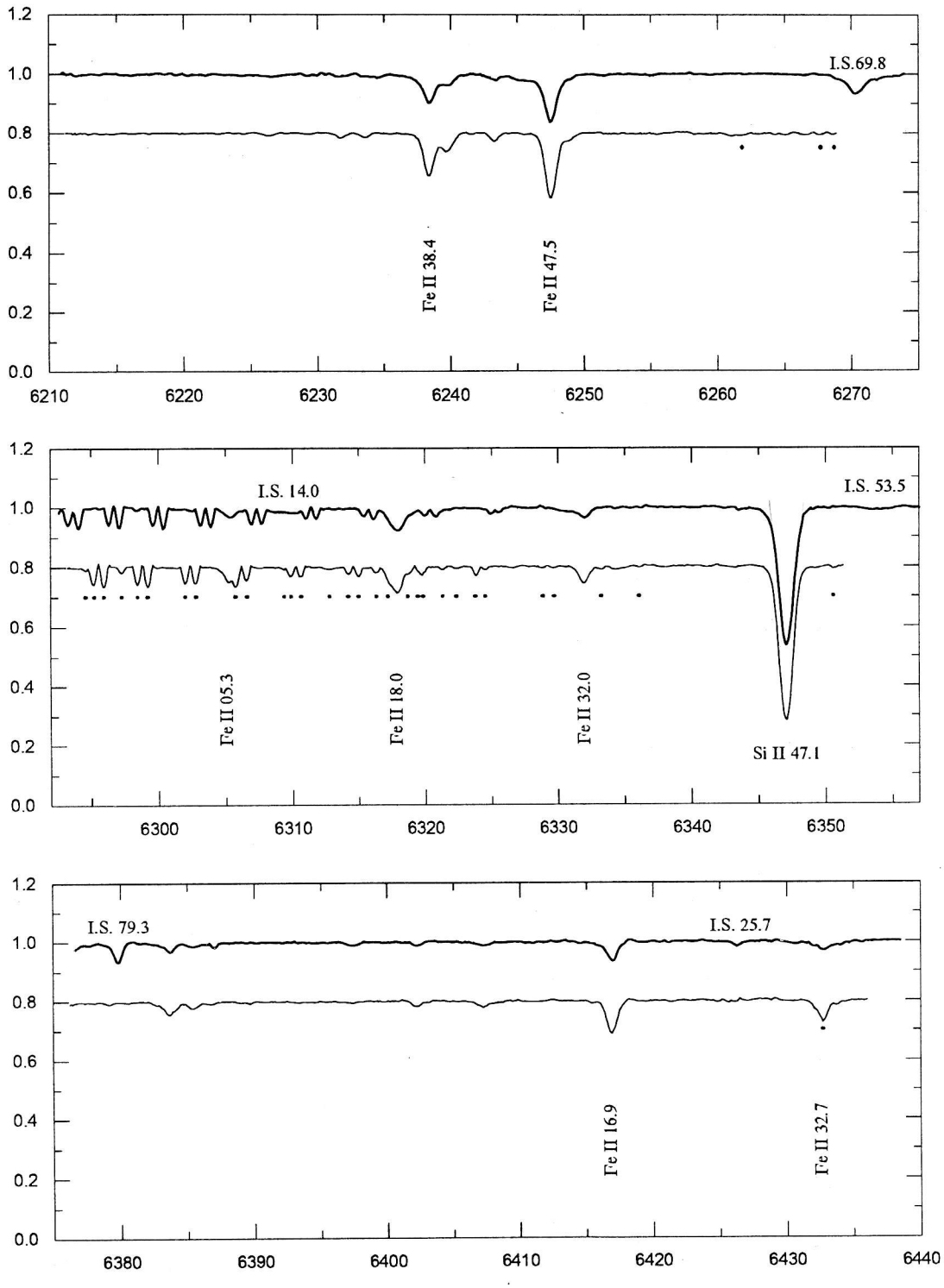

Fig.11 The spectral atlas from 6210 to 6440 A

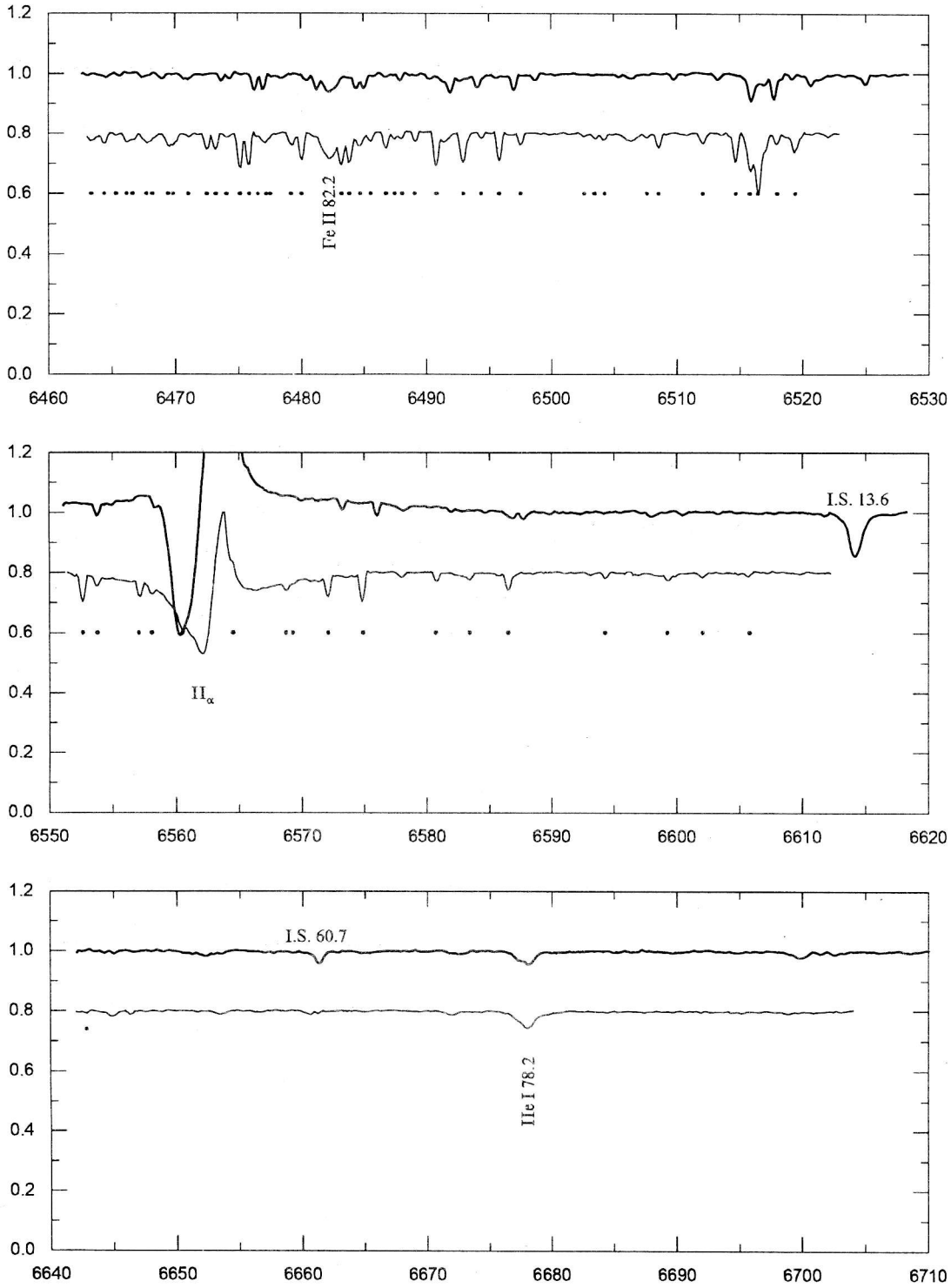

Fig.12 The spectral atlas from 6460 to 6710 A

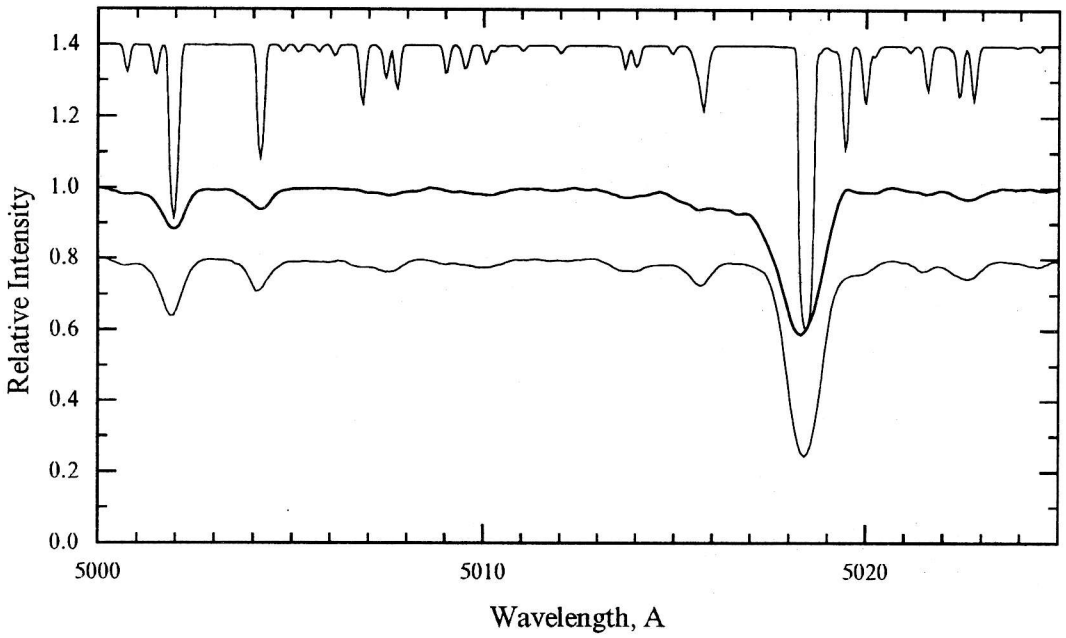

Fig.13 Fragment of atlas and corresponding part of the synthetic spectrum.

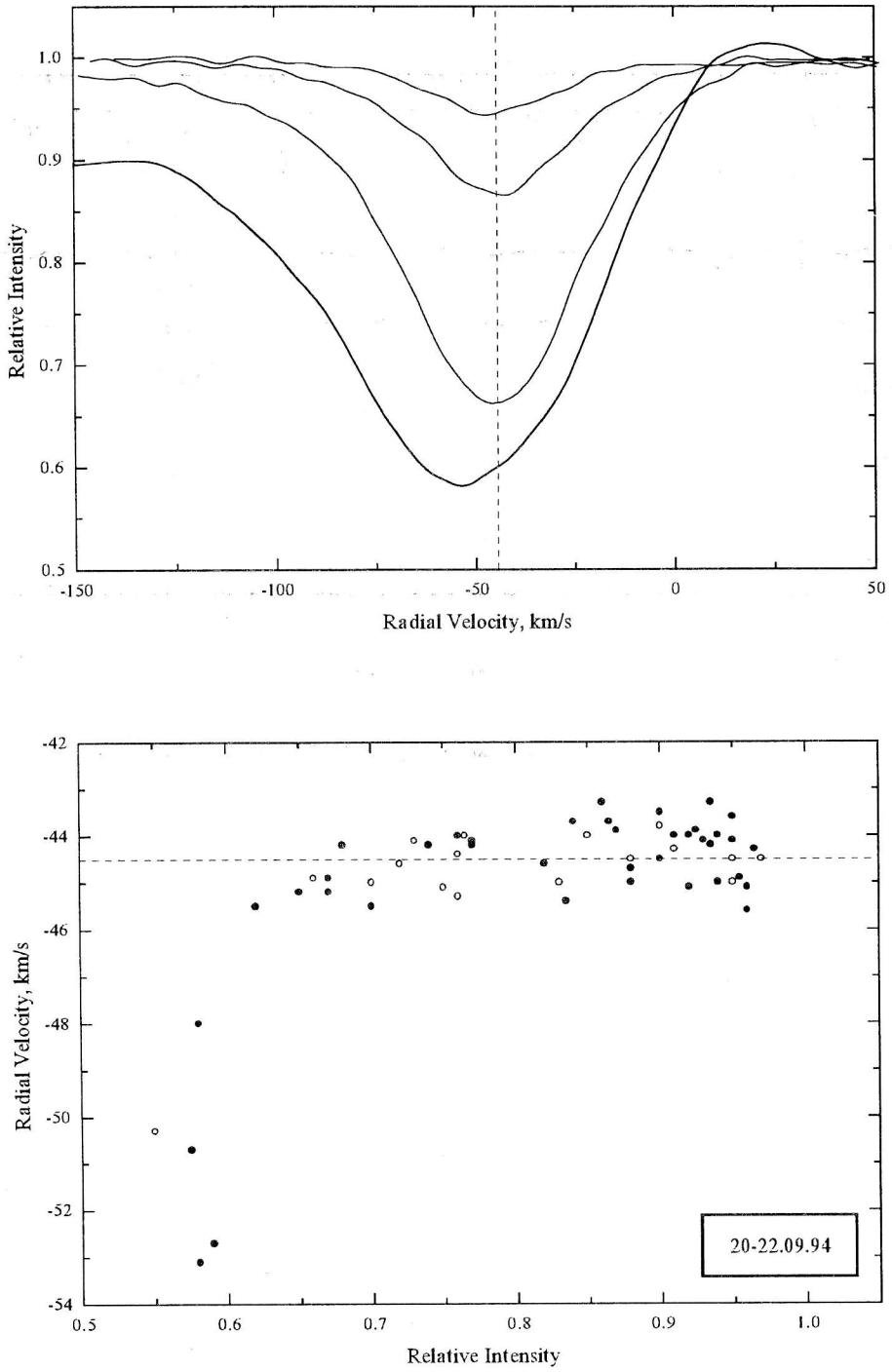

Fig.14 Profiles of FeII lines of different intensity and dependence of radial velocity for the line core upon the line central depth. Filled circles: FeII; open circles: CrII and TiII. Dashed lines are for velocity of the mass center of the star.

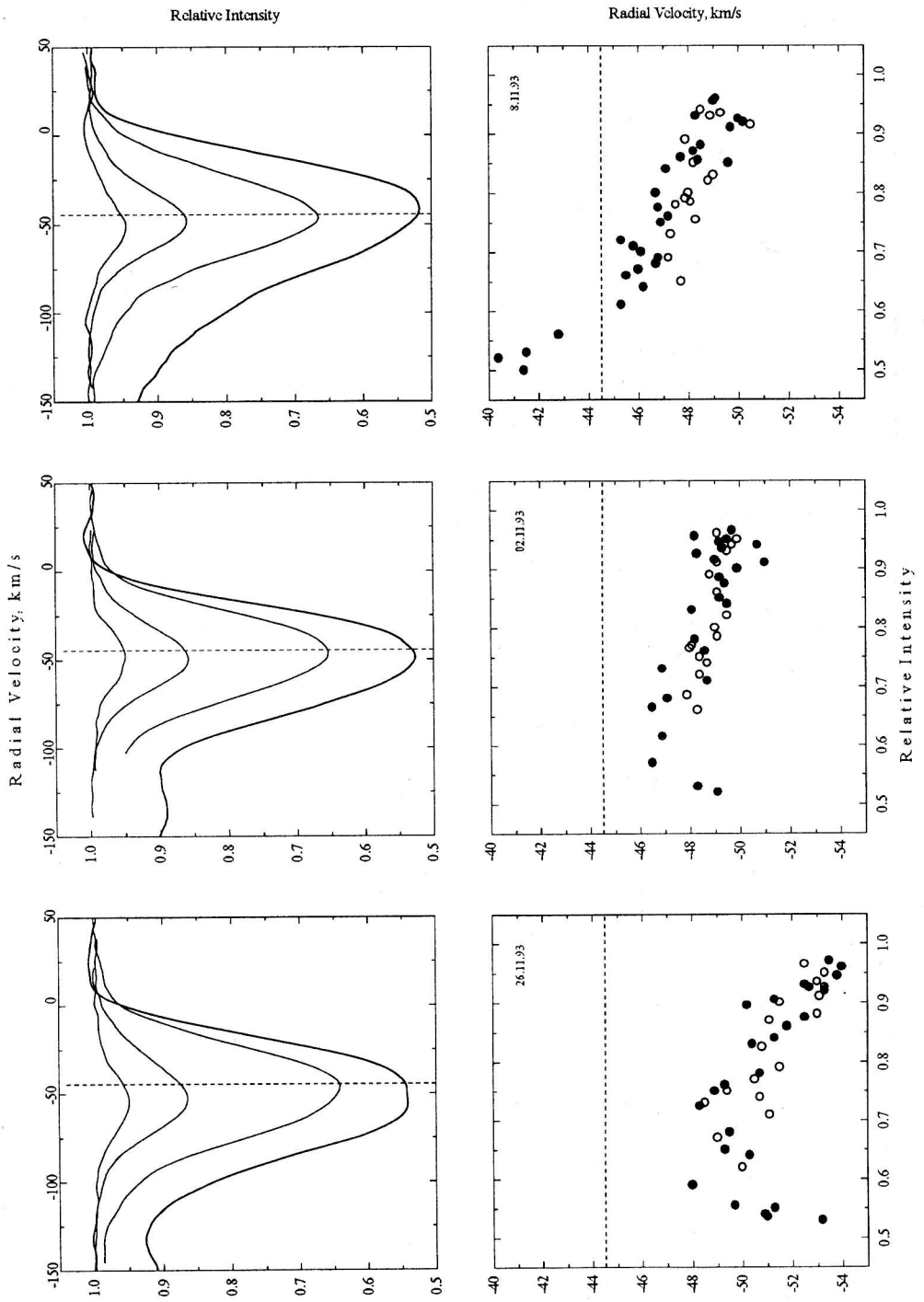

Fig. 15 The same as Fig.14, for three other dates.

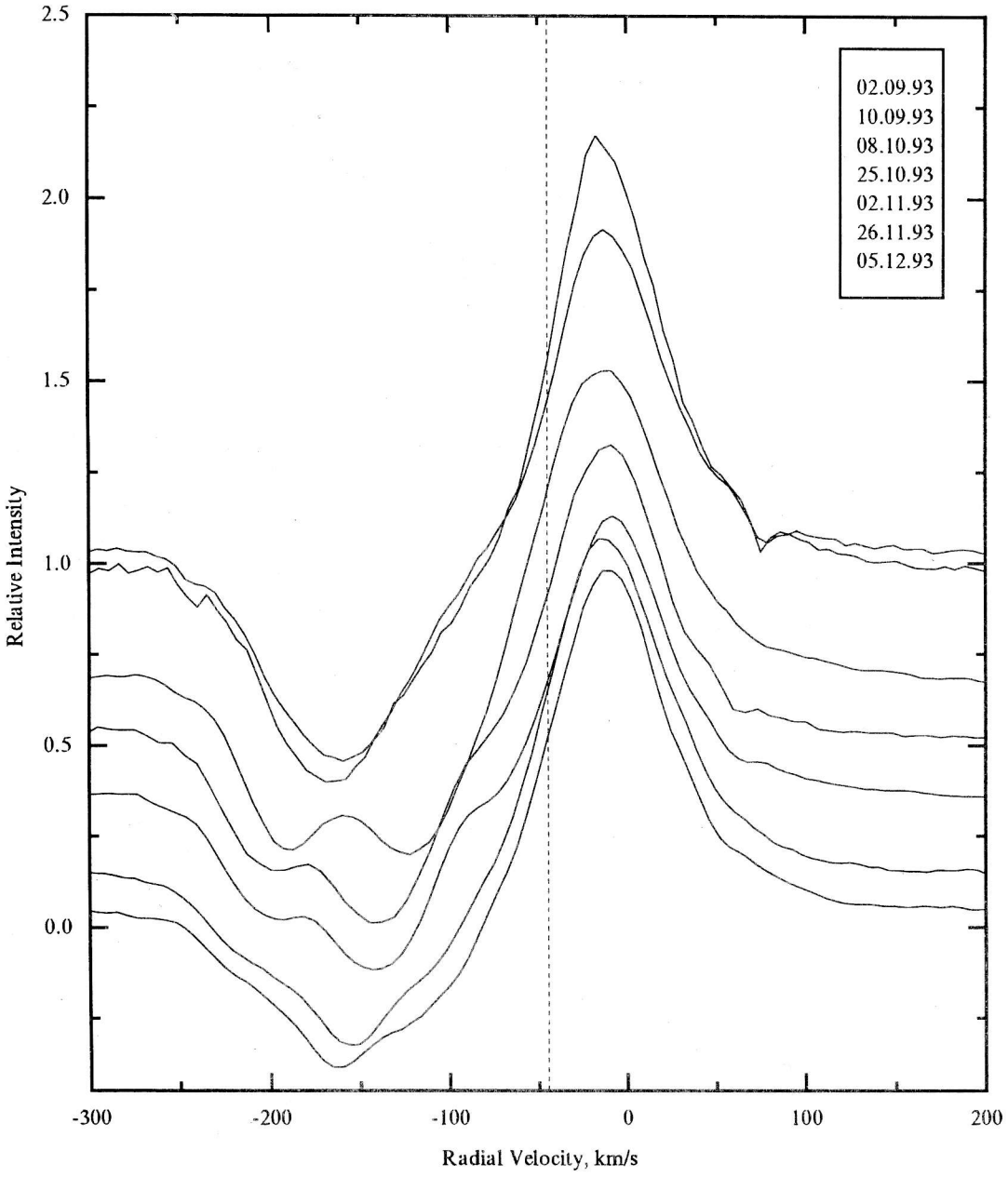

Fig.16 Changing with time in profile H_{α}. Levels of continuous spectrum are separated vertically by time intervals between moments of observations.

I.S.		4428
Mg II	(9)	4433.99
Mg II	(19)	4436.5
Ti II	(40)	4441.7
Ti II	(19)	4443.795
Ti II	(31)	4444.6
Fe II	(187)	4446.2
Fe II	(222)	4449.6
Ti II	(19)	4450.48
Fe II		4451.55
V II	(199)	4453.3
Fe II		4455.26
V II	(199)	4456.5
Fe II	(26)	4461.4
Fe I	(2)	4461.6
Fe II		4461.7
Ti II	(40)	4464.45
Ti II	(146)	4465.7
Cr II		4465.8
Fe I	(2)	4466.6
Ti II	(31)	4468.49
Ti II	(40)	4470.9
He I	(14)	4471.52
Fe II	(37)	4472.92
Fe II	(171)	4474.2
Fe I	(350)	4476.0
Ca II	(6)	4478.7
Mg II	(4)	4481.224
Fe I		4487.2
Ti II	(115)	4488.3
Fe II	(37)	4489.174
Fe II	(37)	4491.398
Ti II	(18)	4493.5
Fe II	(222)	4493.6
Ti II	(18)	4499.6
Ti II	(31).	4501.268
I.S.		4501.8
Ti II	(30)	4506.7
Cr II	(16)	4507.2
Fe II	(213)	4507.2
Fe II	(38)	4508.281
Fe II	(37)	4515.335
Ti I	(42)	4518.0
Ti II	(18)	4518.3
Fe II	(37)	4520.22
Fe II	(38)	4522.63
Ti II	(60)	4524.7
V II	(56)	4528.5
Ti II	(82)	4529.48
TiII(50),FeII(37)		4534.02
Cr II	(39)	4539.6
Fe II	(38)	4541.515
Ti II	(60)	4544.0
Ti II	(30)	4545.1

FeII(38),TiII(82)		4549.54
Ti II	(30)	4552.3
Ba II	(1)	4554.0
Cr II	(44)	4555.0
Fe II	(37)	4555.885
Cr II	(44)	4558.645
Ti II	(50)	4563.755
Cr II	(39)	4565.77
Ti II	(60)	4568.3
Ti II	(82)	4571.97
Fe II	(38)	4576.335
Fe II		4579.5
Fe II	(26)	4580.1
Fe II	(37)	4582.8
Fe II	(38)	4583.835
Cr II	(44)	4588.20
Cr II	(44)	4589.94
Ti II	(50)	4589.94
Cr II	(44)	4592.05
Fe I	(971)	4593.5
Fe II	(38)	4595.7
Fe II	(219)	4598.5
Fe II	(43)	4601.3
Cr II	(44)	4616.62
Cr II	(44)	4618.82
Fe II	(38)	4620.51
Si II		4621.6
Fe II	(186)	4625.91
Fe II	(37)	4629.334
Fe II	(219)	4631.9
Cr II	(44)	4634.072
Fe II	(186)	4635.31
Cr I	(32)	4637.8
Fe II	(25)	4648.9
Fe II	(43)	4657.01
Ti II	(59)	4557.2
Fe II	(146)	4660.9
Ti II	(38)	4662.7
Ti II	(38)	4663.0
Fe II	(44)	4663.7
Fe II	(26)	4665.8
Fe II	(37)	4666.75
Fe II	(25)	4670.19
Sc II	(24)	4670.4
Fe I	(821)	4678.9
Cr II	(177)	4697.6
Mg I	(11)	4703.0
Ti II	(49)	4708.66
He I	(12)	4713.185
S II	(9)	4716.2
I.S.		4726
Fe II	(43)	4731.47
Mg II	(18)	4739.6
Mn II	(5)	4755.72

I.S.		4763.0
Ti II	(48)	4764.5
Mn II	(5)	4764.7
Ti II	(92)	4779.98
Ti II	(17)	4798.5
Ti II	(92)	4805.085
Cr II	(30)	4812.35
S II	(9)	4815.5
Cr II	(30)	4824.136
Fe II	(30)	4833.1
Cr II	(30)	4836.235
Fe II	(30)	4840.0
Fe II		4843.2
Cr II	(30)	4848.248
Mg II	(25)	4851.1
Fe II	(25)	4855.5
Cr II	(30)	4856.2
H_β		4861.332
Cr II	(30)	4864.32
Fe II	(25)	4871.3
Ti II	(114)	4874.0
Cr II	(30)	4876.40
I.S.		4882
Fe II		4883.3
Cr II	(30)	4884.60
Fe I	(318)	4890.8
Fe I	(318)	4891.5
Fe II	(36)	4893.8
Cr II	(190)	4901.7
Fe II		4908.1
Ti II	(114)	4911.19
Cr II	(190)	4912.5
Fe II	(218)	4913.4
Fe I	(318)	4919.0
Fe I	(318)	4920.5
He I	(48)	4921.94
Fe II	(42)	4923.923
Ba II	(1)	4934.1
Fe II		4948.1
Fe II		4948.8
Fe II		4951.58
Cr II		4952.8
Fe II	(168)	4954.0
Fe I	(318)	4957.57
O I	(14)	4967.4
O I	(14)	4967.9
O I	(14)	4968.8
Fe II		4969.4
Fe II		4977.0
Fe II		4984.50
Fe II		4990.5
Fe II	(25)	4991.1
S II	(7)	4991.9
Fe II	(36)	4993.35

Table 1: Lines identification and effective wavelength

Fe II		4999.2
Fe II	(25)	5000.7
Ca II	(15)	5001.5
Fe II		5001.925
Fe II		5004.20
Fe II		5006.8
Fe II		5007.6
Fe II		5009.0
S II	(7)	5009.5
Fe II		5010.1
Ti II	(113)	5013.4
Ti II	(71)	5013.7
S II	(15)	5014.0
He I	(4)	5015.68
Fe II		5015.8
Fe II	(42)	5018.439
O I	(13)	5018.8
O I	(13)	5019.3
Fe II	(168)	5019.5
Ca II	(15)	5020.0
O I	(13)	5020.2
Ca II	(15)	5021.1
Fe II		5021.6
Fe II		5022.6
Fe II		5026.8
Fe II		5030.6
Sc II	(23)	5031.0
S II	(7)	5032.4
Fe II		5032.7
Fe II		5035.71
Si II	(5)	5041.026
Fe II		5045.1
Fe II		5047.6
He I	(47)	5047.7
Si II(5),Si II(5)		5056.06
Fe II		5061.73
Fe II		5065.4
Fe II		5067.9
Fe II		5070.90
Ti II	(113)	5072.3
Fe II		5073.5
Fe II	(205)	5074.0
Fe II		5075.8
Fe II		5082.2
Fe II		5089.2
Fe II		5093.57
Cr II(24),Fe II		5097.27
Fe II	(35)	5100.74
Fe II	(185)	5100.74
Fe II		5106.1
Fe II		5117.0
Fe II		5120.3
Fe II		5123.2
Fe II	(167)	5127.8
Ti II	(86)	5129.155
Fe II	(35)	5132.7
Cr II	(201)	5137.1
Fe II		5143.9
Fe II		5144.4
Fe II		5145.9
Fe II	(35)	5146.1
Fe II		5148.9
Fe II		5149.45
Fe II		5150.6
Fe II		5152.9
Cr II	(24)	5153.5
Ti II	(70)	5154.1
Fe II		5157.4
Fe II		5158.1
Fe II	(167)	5160.8
Mg I	(2)	5167.33
Fe II	(42)	5169.03
Mg I	(2)	5172.69
Fe II		5177.0
Fe II		5177.4
Fe II		5180.3
Mg I	(2)	5183.61
Ti II	(86)	5185.9
Fe II		5186.9
Ti II	(70)	5188.68
Fe II	(49)	5197.58
Fe II		5199.1
Fe II		5203.6
Cr I	(7)	5204.5
Cr I	(7)	5206.0
Cr I	(7)	5208.4
Cr II	(24)	5210.9
Ti II	(103)	5211.5
Fe II		5214.0
Fe II		5215.3
Fe II		5215.8
Fe II		5216.85
Fe II		5218.8
Fe II		5225.3
Ti II	(70)	5226.5
Fe I	(37)	5227.2
Fe II		5227.45
Fe II		5228.8
Cr II	(43)	5232.5
Fe II		5232.8
Fe I	(383)	5232.9
Fe II	(49)	5234.62
Cr II	(43)	5237.32
Fe II		5238.0
Fe II		5239.8
Fe II		5243.2
Cr II	(23)	5246.8
Fe II		5247.95
Fe II		5251.235
Fe II	(41)	5256.9
Fe II		5258.0
Fe II		5260.26
Ti II	(70)	5262.1
Fe II	(52)	5262.3
Mg II	(17)	5264.2
Fe II		5264.2
Fe II		5264.8
Ti II	(103)	5268.6
Fe I	(15)	5269.5
Fe II	(185)	5272.395
Cr II	(43)	5275.0
Fe II	(49)	5276.00
Fe II	(225)	5278.2
Fe II	(184)	5278.9
Cr II	(43)	5280.0
Fe II	(41)	5284.10
Fe II		5291.665
Fe II		5298.8
Mn II	(11)	5299.3
Mn II	(11)	5302.3
Cr II	(24)	5305.9
Fe II		5306.2
Cr II	(43)	5308.4
Cr II	(43)	5313.58
FeII(49),FeII(48)		5316.65
Fe II		5318.1
Cr II	(23)	5318.4
S II	(38)	5320.7
Fe II		5321.8
Fe II		5322.2
Fe I	(553)	5324.2
Fe II	(49)	5325.56
Fe I	(15)	5328.0
O I	(12)	5329.0
O I	(12)	5329.6
O I	(12)	5330.7
Cr II	(43)	5334.865
Ti II	(69)	5336.8
Fe II	(48)	5337.73
Cr II	(43)	5337.8
Fe II		5339.59
S II	(38)	5345.7
Cr II	(24)	5346.1
Cr II	(23)	5346.5
Fe II		5358.9
Fe II	(48)	5362.86
Fe II		5375.8
Ti II	(69)	5381.0
Fe I	(1146)	5383.4
Fe II		5387.07
Fe II		5393.6
Fe II		5393.8
Fe II		5395.86

Table 1 – continued: Lines identification and effective wavelength

Mg II	(24)	5401.1
Fe II		5402.1
I.S.		5404.3
Cr II	(23)	5407.62
Fe II	(184)	5408.8
Fe II	(48)	5414.07
Fe II		5414.8
Ti II	(69)	5418.8
CrII(22),CrII(29)		5419.4
Cr II	(23)	5420.9
Fe I	(1146)	5424.0
Fe II	(49)	5425.245
Fe II		5427.8
S II	(6)	5432.8
Fe II		5442.4
Fe II		5444.4
Fe II		5445.8
I.S.		5449
S II	(6)	5453.8
Cr II	(50)	5455.8
Fe II		5455.9
Fe II		5457.7
Fe II		5466.00
Fe II		5466.92
Fe II		5472.9
Fe II		5473.6
S II	(6)	5473.6
Fe II		5475.8
Cr II	(50)	5478.365
Fe II		5479.4
Fe II		5481.1
Fe II		5482.33
I.S.		5487.3
Fe II		5487.63
Cr II	(50)	5502.1
Fe II		5502.7
Cr II	(50)	5503.2
Fe II		5503.2
Fe II		5506.20
Fe II		5507.1
Cr II	(50)	5508.62
S II	(6)	5509.7
Cr II	(23)	5510.7
Fe II		5510.8
Fe II		5511.1
O I	(25)	5512.7
Fe II	(56)	5525.1
Sc II	(31)	5526.81
Mg I	(9)	5528.4
Fe II		5529.1
Fe II	(224)	5529.9
Fe II		5532.1
Fe II		5534.845

Cr II	(35)	5543.8
Fe II		5544.2
Fe II	(166)	5544.8
Fe II		5548.2
Fe II		5549.0
Fe II		5627.2
Fe II	(57)	5627.5
Fe II		5639.7
S II	(14)	5640.0
S II	(11)	5640.3
Fe II		5643.9
Fe II		5645.41
Fe II		5646.2
S II	(14)	5647.0
Fe II		5648.9
Sc II	(29)	5657.9
Fe II		5657.9
S II	(11)	5660.0
Fe II		5660.1
S II	(11)	5664.7
I.S.		5705.12
Fe II		5726.6
Fe II		5746.6
Fe II		5747.9
I.S.		5778.3
Fe II		5780.2
I.S.		5780.41
Fe II		5783.6
Fe II		5784.4
I.S.		5797.03
Fe II	(163)	5813.7
Fe II		5835.5
Fe II		5842.3
I.S.		5849.79
Fe II		5854.2
Si II	(8)	5868.4
He I	(11)	5875.72
Na I	(1)	5889.95
Na I	(1)	5895.924
Fe II		5952.5
Fe II		5955.7
Si II	(4)	5957.56
Fe II		5961.71
Si II	(4)	5978.93
Fe II	(46)	5991.37
I.S.		6010.9
Fe II		6061.0
Fe II	(46)	6084.10
Cr II	(187)	6089.7
Fe II	(200)	6103.5
I.S.		6113.0
Fe II	(74)	6147.74
Fe II	(74)	6149.25

O I	(10)	6156.0
O I	(10)	6156.8
O I	(10)	6158.184
Fe II	(200)	6175.16
I.S.		6177.1
Cr II	(187)	6179.2
Fe II	(163)	6179.4
Al II	(10)	6231.8
Fe II		6233.5
Fe II	(74)	6238.39
Fe II	(34)	6239.9
Al II	(10)	6243.1
Fe II		6247.4
Fe II	(74)	6247.545
Fe II		6248.9
I.S.		6269.77
Fe II	(200)	6305.31
S II	(19)	6305.5
I.S.		6314
Fe II		6317.4
Fe II		6317.98
Fe II	(199)	6331.96
Si II	(2)	6347.10
I.S.		6353.5
Si II	(2)	6371.36
I.S.		6379.30
Fe II		6383.7
Fe II		6385.5
Ne I	(1)	6402.2
Fe II	(74)	6407.3
Fe II	(74)	6416.93
I.S.		6425.7
Fe II		6425.7
Fe II	(40)	6432.70
Fe II	(199)	6433.8
Fe II	(74)	6456.38
Fe II	(199)	6482.24
Fe II		6491.3
Fe II		6493.1
Fe II		6506.3
Fe II	(40)	6516.1
H_β		6562.81
C II	(2)	6578.1
I.S.		6613.63
I.S.		6660.71
Fe I	(268)	6678.0
He I	(46)	6678.13

Table 1 – continued: Lines identification and effective wavelength